

# T-Explainer: A Model-Agnostic Explainability Framework Based on Gradients

Evandro S. Ortigosa<sup>1</sup>, Fábio F. Dias<sup>2</sup>, Brian Barr<sup>3</sup>, Claudio T. Silva<sup>2</sup>, and Luis Gustavo Nonato<sup>1</sup>

<sup>1</sup>University of São Paulo (ICMC-USP), São Carlos 13566-590, Brazil

<sup>2</sup>New York University, Brooklyn 11201, USA

<sup>3</sup>Capital One, McLean 22102, USA

evortigosa@usp.br, ffd2011@nyu.edu, brian.barr@capitalone.com, csilva@nyu.edu,  
gnonato@icmc.usp.br

## Abstract

The development of machine learning applications has increased significantly in recent years, motivated by the remarkable ability of learning-powered systems to discover and generalize intricate patterns hidden in massive datasets. Modern learning models, while powerful, often exhibit a complexity level that renders them opaque black boxes, lacking transparency and hindering our understanding of their decision-making processes. Opacity challenges the practical application of machine learning, especially in critical domains requiring informed decisions. Explainable Artificial Intelligence (XAI) addresses that challenge, unraveling the complexity of black boxes by providing explanations. Feature attribution/importance XAI stands out for its ability to delineate the significance of input features in predictions. However, most attribution methods have limitations, such as instability, when divergent explanations result from similar or the same instance. This work introduces T-Explainer, a novel additive attribution explainer based on the Taylor expansion that offers desirable properties such as local accuracy and consistency. We demonstrate T-Explainer's effectiveness and stability over multiple runs in quantitative benchmark experiments against well-known attribution methods. Additionally, we provide several tools to evaluate and visualize explanations, turning T-Explainer into a comprehensive XAI framework.

**Keywords:** Black-box models, explainable artificial intelligence, XAI, interpretability, local explanations.

## 1 Introduction

Artificial Intelligence is not a vision for the future. It is our present reality. Terms such as Neural Networks, Machine Learning, Deep Learning, and other facets of the Artificial Intelligence universe have seamlessly shifted from futuristic concepts to near-ubiquitous elements in our daily discourse. The confluence of recent advances in hardware processing capabilities, abundant data accessibility, and refined optimization algorithms has facilitated the creation of intricate and

non-linear machine learning models [12]. In the contemporary landscape, these models have achieved unprecedented performance levels, surpassing what was deemed inconceivable just a few years ago, outperforming human abilities and previously known methods in central research areas [42, 48].

The complex non-linear structures and vast number of parameters inherent in such models pose a challenge to transparent interpretation and comprehension of the rationale behind their decisions. This characteristic transforms those models into black boxes in which one can discern only what inputs are provided and what outputs are produced without a clear understanding of the internal decision-making processes [13]. Lack of transparency causes trust-related apprehensions, hindering the effective deployment of more powerful machine learning models in critical applications [2, 6, 34]. Furthermore, it poses challenges in adhering to emerging regulatory norms observed in numerous countries [16, 44], thereby complicating compliance efforts.

Widely used machine learning models are impenetrable as far as simple interpretations of their mechanisms go [13]. In this context, Explainable Artificial Intelligence (XAI) has emerged to address the challenges outlined above, seeking to provide human-understandable insights into the complexities of inherently challenging models. Significantly, the field of explainability has progressed with the introduction of innovative methodologies and research has focused on discerning the strengths and limitations of XAI models [2].

Feature attribution/importance methods are particularly relevant, as they are currently the most common explanation type [33, 46]. Such methods aim to quantify the contribution of individual input variables to predictions made by black-box models, providing local insights about model reasoning [34]. While feature attribution methods prove valuable, they have drawbacks that diminish trust and confidence in their application. For example, different methods can result in distinct explanations for the same data instances, making it difficult to decide which outcome to believe [46]. Moreover, many well-known methods, including SHAP [30] and LIME [36] suffer

instability, producing different explanations from different runs on a fixed machine learning model and dataset [14].

An explanation method must produce consistent explanations in multiple runs on the same and similar instances to be considered stable. Stability is a fundamental objective in XAI, as explainability methods that generate inconsistent explanations for similar instances (or even for the same instance) are challenging to trust. If explanations lack reliability, they are essentially useless. Therefore, to be considered reliable, an explanation model must, at a minimum, exhibit stability [5].

In this work, we introduce T-Explainer, a novel post-hoc explanation method that relies on the solid mathematical foundations of Taylor expansion to perform local and model-agnostic feature importance attributions. T-Explainer is a local additive explanation technique with desirable properties such as local accuracy, missingness, and consistency [30]. Furthermore, T-Explainer is deterministic, guaranteeing stable results across multiple runs and providing consistent explanations for similar instances.

We conducted several quantitative comparisons against well-known feature attribution methods using controlled synthetic and real-world datasets to evaluate the quality and usefulness of the T-Explainer explanations. Our evaluations focused on consistency, continuity, and correctness of the content explanation [33]. As a result of such an extensive evaluation process, we implemented a suite of quantitative metrics to evaluate different dimensions of feature importance explainers. These metrics were incorporated into the T-Explainer package, making it not just another XAI method but a comprehensive XAI framework.

In summary, the main contributions of this work are as follows.

- **T-Explainer**, a stable model-agnostic local additive attribution method. It faithfully approximates the local behavior of black-box models using a deterministic optimization procedure, enabling reliable and trustworthy interpretations.
- A comprehensive set of comparisons against well-known local feature attribution methods using multiple quantitative **metrics**, aiming to evaluate stability and faithfulness.
- A Python **framework** that integrates T-Explainer with other explainability tools, making the proposed method easy to use and assess in different applications. The T-Explainer, evaluation metrics, datasets, and all related materials are available online.<sup>1</sup>

## 2 Related work

Several XAI techniques have been proposed to deal with black-box models, either locally or globally [46]. To contextualize our contributions, we focus the following discussion on post-hoc feature importance/attribution methods [23, 51].

A more comprehensive discussion about XAI can be found in several surveys summarizing existing approaches and their properties [2, 6, 28, 34] and metrics to evaluate explanation methods [3, 33, 52].

Breiman [13] proposed one of the first approaches to identify the features that most impact the predictions of a model. Breiman’s solution is model-specific (Random Forests) and involves permuting the values of each feature and computing the model loss. Given the feature independence assumption, the method identifies the most important features by prioritizing those that contribute the most to the overall loss.

More general approaches, the so-called model-agnostic techniques, can (theoretically) operate with any machine learning model, regardless of the underlying algorithm or architecture. In this context, LIME (Local Interpretable Model-agnostic Explanations) [36], SHAP (SHapley Additive exPlanations) [30], and their variants [34] are model-agnostic methods widely employed to explain machine learning models’ behavior in healthcare [15], financial market [18], and engineering [24] applications.

Although widely used, LIME and SHAP have significant drawbacks that require care when using such techniques. For example, LIME lacks theoretical guarantees about generating accurate simplified approximations for complex models [2]. Moreover, different simplified models can be fitted depending on the random sampling mechanism used by LIME, which can lead to instability to small data perturbation and, sometimes, entirely different explanations by just running the code multiple times [5].

SHAP has a solid theoretical foundation derived from game theory that grants SHAP desirable properties such as local accuracy, missingness, and consistency [30]. However, the exact computation of SHAP values is NP-hard, demanding Monte Carlo sampling-based approximations [34, 46], which introduces instability similar to the LIME method, even in model-specific variants [31, 34]. To avoid instability, deterministic versions of LIME [53], optimization [25], and learning-based [41] approaches have been proposed, but at the price of increasing the number of parameters to be tuned.

Gradient-based methods are another important family of explanation approaches. Those methods attribute importance to each input feature by analyzing how their changes affect the model’s output, relying on gradient decomposition to quantify those effects. Vanilla Gradient [40] introduced the use of gradients in feature attribution tasks. The method computes partial derivatives at the input point  $x$  with a Taylor expansion around a different point  $x'$  and a remainder bias term, for which neither is defined [7]. Monte Carlo sampling can be used to estimate derivatives, but it makes the Vanilla Gradient suffer from instability and noise within the gradients.

LRP (Layer-wise Relevance Propagation) [7] identifies properties related to the maximum uncertainty state of predictions by redistributing an importance score back to the model’s input layer. The Integrated Gradients method [45] quantifies the feature importance by integrating gradients from the target input to a baseline instance. Input  $\times$  Gradient highlights in-

<sup>1</sup> Available at [https://github.com/evortigosa/EXplainable\\_AI](https://github.com/evortigosa/EXplainable_AI)

fluential regions in the input space by computing the features' element-wise product and corresponding gradients from the model's output [34]. DeepLIFT (Deep Learning Important FeaTures) [39] is based on LRP's importance scores to measure the difference between the model's prediction of a target input and baseline instance.

The stability of gradient-based methods depends on gradient propagation, the model's complexity, and the baseline choice [39]. Additionally, most of those methods are designed specifically for explanation tasks in Neural Networks and other models with differentiable parameters.

T-Explainer differs from the methods described above in three main aspects: (i) it is deterministic, T-Explainer defines an optimization procedure based on finite differences to estimate partial derivatives, thus being stable by definition; (ii) T-Explainer relies on just a few hyperparameters, rendering it easy to use; and (iii) T-Explainer is not dependent on baselines. Moreover, T-Explainer is built on the solid mathematical foundations of the Taylor expansion, which naturally endows it with desirable properties similar to those of SHAP. Although T-Explainer, in theory, is designed to be applied to differentiable models, we show experimentally that it also produces interesting results operating with non-differentiable models, which makes T-Explainer more flexible than previous gradient-based methods.

### 3 The T-Explainer

In this Section, we introduce the theoretical foundations, properties, and computational aspects of the T-Explainer method.

Let  $\mathbf{X}$  be a multidimensional dataset where each data instance  $\mathbf{x} = (x_1, \dots, x_n) \in \mathbf{X}$  is a vector in  $\mathbb{R}^n$  and  $f$  be a machine learning model. For simplicity, let's assume that  $f$  is a binary classification model trained on  $\mathbf{X}$ , that is,  $f(\mathbf{x}) \in (0, 1)$  accounts for the probability of  $\mathbf{x}$  belonging to class 1, and  $(1 - f(\mathbf{x}))$  is the probability of belonging to class 0. All the following reasoning can be extended to regression models.

The model  $f$  can be seen as a real-valued function:

$$f : \mathbf{X} \rightarrow (0, 1) \subset \mathbb{R} \quad (1)$$

As a real function,  $f$  can be linearly approximated through first-order Taylor expansion:

$$f(\mathbf{x} + \mathbf{h}) \approx f(\mathbf{x}) + \nabla f(\mathbf{x}) \cdot \mathbf{h} \quad (2)$$

where  $\mathbf{h}$  is a displacement vector corresponding to a small neighborhood perturbation of  $\mathbf{x}$  and  $\nabla f(\mathbf{x})$  is the gradient (linear transformation) of  $f$  in  $\mathbf{x}$ , given by:

$$\nabla f(\mathbf{x}) = \left[ \frac{\partial f(\mathbf{x})}{\partial x_1}, \dots, \frac{\partial f(\mathbf{x})}{\partial x_n} \right]. \quad (3)$$

The  $i$ -th gradient element corresponds to the partial derivative of  $f$  concerning the  $i$ -th attribute of  $\mathbf{x}$ . Note that the gradient

of  $f$  in  $\mathbf{x}$  corresponds to the Jacobian matrix when  $f$  is a real-valued function. The dot product between the gradient and the displacement vector  $\mathbf{h}$  is a linear map from  $\mathbb{R}^n$  to  $\mathbb{R}$ , well known as the best linear approximation of  $f$  in a small neighborhood of  $\mathbf{x}$ . Therefore, the gradient can be used to analyze how small perturbations in the input data affect the model output. The right side of Equation 2 is a linear equation that approximates the behavior of  $f$  near  $\mathbf{x}$ , and because it is a linear mapping, it is naturally interpretable. In other words, the gradient of a model  $f$  can be used to generate explanations.

The formulation above resembles the Vanilla Gradient [40] Taylor expansion-based procedure to compute saliency maps. The difference is that, in our case, the attributions are not dependent on class information and do not rely on further parameters specific to the model's architecture. In addition, T-Explainer differs from previous gradient-based methods by relying on additive modeling and a deterministic optimization procedure to approximate gradients, as detailed below.

Let  $\mathbf{h} = \mathbf{z}' \in \mathbb{R}^n$  be a perturbation in  $\mathbf{x}$ , that is,  $\mathbf{x}' = \mathbf{x} + \mathbf{z}'$  is a point in a small neighborhood of  $\mathbf{x}$ . The T-Explainer is defined as an additive explanation modeling  $g_{\mathbf{x}}$ , given by:

$$g_{\mathbf{x}}(\mathbf{z}') = \phi_0 + \sum_{i=1}^n \phi_i z'_i \quad (4)$$

where  $\phi_0 = \mathbb{E}[f(\mathbf{X})]$  represents the expected prediction value, and  $\phi_i = \frac{\partial f(\mathbf{x})}{\partial x_i}$ . The prediction expected value is a statistical value that is not trivial to estimate for an arbitrary dataset. In practice, it is computed through the average model output across the training dataset  $\mathbf{X}$  when the feature values  $\mathbf{X}_i$  are unknown. Specifically, it does not mean that  $\mathbf{X}_i = 0$ ; it means we do not know the value of  $\mathbf{X}_i$ . Therefore, its distribution is estimated based on the data by taking the mean value and then averaging the predicted probabilities for each label. As a fundamental property of additive explanations, Equation 4 approximates the original predicted value  $f(\mathbf{x})$  locally by summing its feature importances [30].

The explanation model  $g_{\mathbf{x}}$  is a local attribution method, i.e., there is a  $g_{\mathbf{x}}$  for each  $\mathbf{x}$ . By definition, T-Explainer is an *additive feature attribution method*, as defined by Lundberg and Lee [30], which means that the importance value attributed to each feature can reconstruct the model prediction by adding those importance values. The coefficient  $\phi_i$  indicates the feature attribution/importance of the  $i$ -th attribute to the prediction made by  $f$  in  $\mathbf{x}$ . In T-Explainer, the feature attribution  $\phi_i$  has a simple and intuitive geometric interpretation, corresponding to the projection of  $\nabla f(\mathbf{x})$  on the  $i$ -th feature axis. Therefore, the more aligned the gradient  $\nabla f(\mathbf{x})$  and the  $i$ -th axis of the feature space, the more important the  $i$ -th feature is to the decision made by  $f$ .

#### 3.1 T-Explainer Properties

According to Lundberg and Lee [30], a “good” explanation method must have three important properties, namely, *Local*

*Accuracy, Missingness, and Consistency.* In the following, we show that T-Explainer approximates *Local Accuracy* while holding *Missingness* and *Consistency*.

### 3.1.1 Local Accuracy

The local accuracy property, as defined by Lundberg and Lee [30], states that if  $f(\mathbf{x} + \mathbf{z}') = g_{\mathbf{x}}(\mathbf{z}') = \phi_0 + \sum_{i=1}^n \phi_i z'_i$ , then  $g_{\mathbf{x}}$  has the local accuracy property. The T-Explainer does not fully satisfy this property but instead approximates it. By construction, we have the following:

$$f(\mathbf{x} + \mathbf{z}') \approx g_{\mathbf{x}}(\mathbf{z}') = \phi_0 + \sum_{i=1}^n \phi_i z'_i \quad (5)$$

and, from the Taylor expansion remainder theorem [32], there is an upper bound to the approximation error given by:

$$f(\mathbf{x} + \mathbf{z}') - g_{\mathbf{x}}(\mathbf{z}') = O(\|\mathbf{z}'\|^2). \quad (6)$$

### 3.1.2 Missingness

The missingness property states that if a feature  $x_i$  has no impact on the model decision, then  $\phi_i = 0$  [30]. In our context, a feature  $i$  having no impact on  $f$  means that  $f$  does not vary (increase or decrease) when only the  $i$ -th feature is changed (otherwise, the feature would impact the model decision). In other words,  $f(x_1, \dots, x_i + z'_i, \dots, x_n) - f(x_1, \dots, x_i, \dots, x_n) = 0$ , thus, there is no variation in the  $i$ -th direction and the partial derivative  $\phi_i = \frac{\partial f(\mathbf{x})}{\partial x_i} = 0$ , ensuring that the T-Explainer holds the missingness property.

### 3.1.3 Consistency

Let  $f$  and  $\tilde{f}$  be two binary classification models. Let us use the notation  $\mathbf{x}' \setminus i$  to indicate that the  $i$ -th feature is disregarded in any perturbation of  $\mathbf{x}$  ( $z'_i = 0$  in any perturbation, so  $x'_i \setminus i = x_i$ ). An explanation method is consistent if (see Lundberg and Lee [30]), fixing  $\mathbf{x}$ ,  $\tilde{f}(\mathbf{x}') - \tilde{f}(\mathbf{x}' \setminus i) > f(\mathbf{x}') - f(\mathbf{x}' \setminus i)$  implies  $\phi_i(\tilde{f}) > \phi_i(f)$ . Suppose that  $\tilde{f}(\mathbf{x}') - \tilde{f}(\mathbf{x}' \setminus i) > f(\mathbf{x}') - f(\mathbf{x}' \setminus i)$  holds in a small neighborhood of  $\mathbf{x}$ , in particular,

$$\begin{aligned} \tilde{f}(x_1 + z'_1, \dots, x_i + z'_i, \dots, x_n + z'_n) - \\ \tilde{f}(x_1 + z'_1, \dots, x_i, \dots, x_n + z'_n) > \quad (7) \\ f(x_1 + z'_1, \dots, x_i + z'_i, \dots, x_n + z'_n) - \\ f(x_1 + z'_1, \dots, x_i, \dots, x_n + z'_n) \end{aligned}$$

for  $z'_i \in (-\delta, 0) \cup (0, \delta)$ .

Define  $\tilde{s}(z'_i) = \frac{\tilde{f}(\mathbf{x}') - \tilde{f}(\mathbf{x}' \setminus i)}{z'_i}$  and  $s(z'_i) = \frac{f(\mathbf{x}') - f(\mathbf{x}' \setminus i)}{z'_i}$ , from Equation 7 we know that  $\tilde{s}(z'_i) > s(z'_i)$  for  $z'_i \in (-\delta, 0) \cup (0, \delta)$ . Assuming that  $\tilde{f}$  and  $f$  are differentiable in  $\mathbf{x}$ , then  $\lim_{z'_i \rightarrow 0} \tilde{s}(z'_i) = \frac{\partial \tilde{f}(\mathbf{x})}{\partial x_i}$  and  $\lim_{z'_i \rightarrow 0} s(z'_i) = \frac{\partial f(\mathbf{x})}{\partial x_i}$  exist, thus, from the *Limit Inequality Theorem*:

$$\phi_i(\tilde{f}) = \frac{\partial \tilde{f}(\mathbf{x})}{\partial x_i} > \frac{\partial f(\mathbf{x})}{\partial x_i} = \phi_i(f) \quad (8)$$

showing that the T-Explainer holds the consistency property (the *Limit Inequality Theorem* ensures that, given two functions  $\tilde{s}, s : (a, c) \cup (c, b) \subset \mathbb{R} \rightarrow \mathbb{R}$ , if  $\tilde{s}(x) > s(x)$  for all  $x \in (a, c) \cup (c, b)$  and the limits  $\lim_{x \rightarrow c} \tilde{s}(x) = A$  and  $\lim_{x \rightarrow c} s(x) = B$  exist, then  $A > B$ ).

According to Lundberg and Lee [30], the Shapley-based explanation is the unique possible additive feature attribution model that (theoretically, see Hooker et al. [21]) satisfies *Local Accuracy*, *Missingness*, and *Consistency* properties. As demonstrated above, T-Explainer approximates *Local Accuracy* while holding *Missingness* and *Consistency*. Therefore, the T-Explainer is one of the few XAI methods that approximate SHAP theoretical guarantees.

## 3.2 T-Explainer: Computational Aspects

Figure 1 illustrates the step-by-step pipeline of T-Explainer for feature attribution. Computing the gradient of a known real-valued function is (theoretically) simple, demanding that the partial derivatives of the function be taken. However, we need to calculate the partial derivatives of an arbitrary black-box model  $f$ , which was previously trained and has complex internal mechanisms. To that end, we perturb the instance  $\mathbf{x}$  attribute-wise and compute the respective change in the model’s output, approximating the partial derivatives through centered finite differences [27]:

$$FD_{f(\mathbf{x})} = \frac{f(\mathbf{x} + \mathbf{h}) - f(\mathbf{x} - \mathbf{h})}{2\|\mathbf{h}\|}. \quad (9)$$

Finite differences are well-established approaches to approximate differential equations, replacing the derivatives with discrete approximations (such transformation results in computationally feasible systems of equations) [27]. Specifically, we rely on the centered finite difference because that approach averages two one-sided perturbations of each attribute, resulting in a second-order accurate approximation with an error proportional to  $\|\mathbf{h}\|^2$  [27]. The centered finite difference approximation of the partial derivatives demands establishing the magnitude of the perturbation  $\mathbf{h}$ . The displacement  $\mathbf{h}$  must be small enough to generate a perturbation close to the input data  $\mathbf{x}$ . By definition, the derivatives of  $f$  are computed by making  $\mathbf{h} \rightarrow 0$  in Equation 9. In other words, we have to set  $\mathbf{h}$  to a small value.

In practice, if  $\mathbf{h}$  is too small, it can generate significant round-off errors or singularity cases. However, if  $\mathbf{h}$  is too large, it can lead to truncation errors and inappropriate approximations. To our knowledge, there is no closed solution to determine an optimum value of  $\mathbf{h}$ . To solve this issue, we developed a  $\mathbf{h}$  optimizer method based on a binary search that minimizes a *mean squared error* (MSE) cost function. The method runs over the  $[h_{min}, h_{max}]$  interval, searching for an optimal  $\mathbf{h}$  to produce a good approximation of  $f(\mathbf{x})$  from Equation 2. We set  $h_{min}$  with the minimum distance between any two

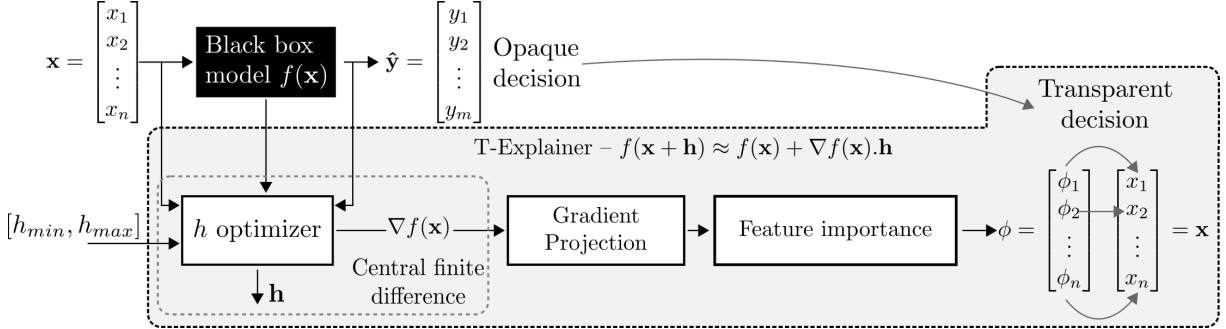


Figure 1: T-Explainer pipeline.

instances on the dataset, i.e.,  $h_{min} = \min_{i,j=1}^n \|\mathbf{x}_i - \mathbf{x}_j\|$ ,  $\forall i \neq j, \mathbf{x}_i, \mathbf{x}_j \in \mathbf{X}$ . The optimization method is formulated as follows.

$$\nabla f(\mathbf{x}) = \arg \min_{\mathbf{h} \in [h_{min}, h_{max}]} \mathcal{L}(f, \mathbf{h}, \epsilon_{\mathbf{x}}) + \theta(\nabla f_{\mathbf{x}}) \quad (10)$$

where  $\mathcal{L}$  is the cost function (MSE in our case),  $\nabla f_{\mathbf{x}}$  represents the approximated value of the gradient  $\nabla f(\mathbf{x})$  in each iteration of the  $\mathbf{h}$  optimizer algorithm computing the method in Equation 9,  $\epsilon_{\mathbf{x}}$  is the upper limit of the cost threshold bound by  $(h_{min})^2$  [27], and  $\theta$  is a method that ensures the numerical stability of the optimization process by checking if  $\nabla f(\mathbf{x})$  comes from a non-singular (or full-rank) Jacobian matrix.

In the presence of a singular matrix, perturbation methods such as finite differences suffer from numerical instability. This instability can lead to inaccurate approximations of the Jacobian, making it unreliable for further calculations or updates. In addition, a singular or rank-deficient Jacobian indicates that some input features or dimensions are linearly dependent, and this is problematic because it means that the model is not fully sensitive to certain input variations, leading to poor sensitivity analysis. Specific to the context of our optimizer, a singular Jacobian leads to a failure in convergence, propagating errors that lead the explainer to output one-hot-like feature importance vectors. Therefore,  $\theta$  rejects  $\mathbf{h}$  when it results in a singular (or rank-deficient) Jacobian.

It is important to highlight that local perturbations must preserve the normalization range of the data to avoid model extrapolations [21]. Further details about the optimization procedure are given in the Appendix. This approach can find the gradient  $\nabla f(\mathbf{x})$  of a binary-class model or even the entire Jacobian related to all the model’s output probabilities. Once the gradient is estimated at  $\mathbf{x}$ , the importance of each attribute is computed as  $\phi_i = \frac{\partial f(\mathbf{x})}{\partial x_i}$ .

The explanations must remain consistent with the model’s behavior in the instance’s locality to ensure meaningful interpretability. Through the  $\mathbf{h}$  optimization process, T-Explainer attributes feature importance using Taylor’s expansion for each instance tailored to its local characteristics. In other words, the T-Explainer is designed primarily as a local ex-

plainer. According to Ribeiro et al. [36], simultaneously achieving local and global fidelity in XAI is challenging because the aggregation of local explanations to estimate global feature importance could be ineffective. After all, local explanations are instance-specific and often inconsistent with global explanations. However, the adaptive  $\mathbf{h}$  optimization strategy of T-Explainer is flexible enough to be extended and generate aggregated views while preserving local relationships, enhancing consistent and interpretable explanations at local and global levels.

### 3.2.1 Handling Categorical Data

All the considerations outlined in the T-Explainer’s theoretical foundations (see The T-Explainer Section) assume that the attributes are continuous numerical data. However, most datasets are not limited to numerical data but also encompass categorical (nominal or qualitative) features. Handling categorical data is challenging, as many learning models cannot directly process nominal features, demanding numerical conversions. Different approaches can be applied to encode categorical values as numerical representations, including the well-known one-hot encoding [37].

Numerical encodings introduce challenges for XAI methods, particularly those based on gradients. Nominal values represented with one-hot encode become binary constant values (zeros and ones), thus being discontinuous attributes where partial derivatives can not be properly estimated, inducing the explainer to erroneously attribute null importance to features that may significantly impact the prediction.

T-Explainer has a modular design that enhances flexible additions or improvements in functionalities. To address the challenges of categorical features, we implemented a mechanism to handle one-hot encoded columns into the T-Explainer framework. Once the user identifies the one-hot encoded categorical attributes, a procedure transforms them into intervals through continuous perturbations. Specifically, the values 0 and 1 (resulting from one-hot encoding) are uniformly perturbed with displacement in the interval  $\delta \in (-0.5, 0.5)$ , creating a range of values around 0 and 1, simulating a continuous set of values around these two values.

The continuity induction procedure is performed on a copy of the training dataset, with the perturbed columns normalized

to the same interval of the numerical features (typically in the  $[0, 1]$  range). After that, transfer learning is applied to a copy of the original model, fitting it with the perturbed training dataset (the categorical fitted model). Finally, the T-Explainer runs on the newly trained model. In summary, predictions of instances holding categorical features are explained using the T-Explainer’s core implementation. However, we incorporated a preliminary layer in T-Explainer’s pipeline to handle categorical data.

The perturbation radius  $\delta$  can affect the accuracy of the categorical fitted model, making it disagree with the original model. However, the disagreement varies according to the training data. In our experiments, the proposed transformation of categorical attributes to numerical ones does not significantly impact the accuracy of the categorical fitted model for perturbations in small intervals. We fixed  $\delta = 0.1$  as the perturbation radius, which ensured accuracy preservation.

## 4 Quantitative Metrics

A common drawback of research proposing XAI methods is a lack of clarity on the use of quantitative evaluations [33]. Most proposals rely on visual inspections or simplified human-centered case studies to check whether an explanation “looks reasonable.” However, such anecdotal strategies are prone to subjectivities and do not allow for formal comparisons between explanation methods, which is insufficient to ensure a robust verification of explanations’ consistency, continuity, and correctness [33]. Evaluation in XAI evolved significantly in the past few years, and this Section describes the evaluation metrics integrated into the T-Explainer framework.

A stability metric measures the robustness or sensitivity of an explainer when exposed to slightly different versions of an original input sample. *Relative Input Stability* (RIS) and *Relative Output Stability* (ROS) [3] are metrics used to evaluate the stability of local explanations to changes in input data and output prediction probabilities, respectively, based on the “relative stability” formulation that applies normalized distances allowing direct comparisons between different feature importance methods. We followed the theoretical definitions of RIS and ROS defined by Agarwal et al. [3].

Given  $\mathcal{N}_x$  a neighborhood of perturbed samples  $x'$  around an original input instance  $x$ , with  $e_x$  and  $e_{x'}$  representing the attribution vectors explaining  $x$  and  $x'$ , and  $f(x)$  and  $f(x')$  the output prediction probabilities of  $x$  and  $x'$ , RIS and ROS metrics are defined as:

$$\text{RIS}(x, x', e_x, e_{x'}) = \max_{x'} \frac{\| \frac{e_x - e_{x'}}{e_x} \|_p}{\max(\| \frac{x - x'}{x} \|_p, \epsilon_c)} \quad \text{and} \quad (11)$$

$$\text{ROS}(x, x', e_x, e_{x'}) = \max_{x'} \frac{\| \frac{e_x - e_{x'}}{e_x} \|_p}{\max(\| \frac{f(x) - f(x')}{f(x)} \|_p, \epsilon_c)} \quad (12)$$

$\forall x' \in \mathcal{N}_x$ ,  $\hat{y}_x = \hat{y}_{x'}$ , with  $p$  defining the  $l_p$  norm used to measure the changes and  $\epsilon_c > 0$  as a small value threshold

to avoid zero division. The higher the RIS or ROS values, the more unstable the method is related to input or output prediction perturbation.

We identified some issues that prevented us from using the implementations of Agarwal et al. [3]. Notably, their framework lacks flexibility for incorporating novel explainers beyond those included in OpenXAI, and the separate execution of RIS and ROS metrics reduces their comparability due to differences in the perturbed samples drawn from normal distributions. In contrast, our T-Explainer framework offers a flexible Python module that can be readily extended to assess multiple feature attribution methods while computing RIS and ROS in parallel.

Previously, the selection of perturbed samples satisfying  $\hat{y}_x = \hat{y}_{x'}$  was performed randomly, with no guarantee that a sufficient number of samples would be retained – particularly near the model’s decision boundaries. We solved this limitation by sampling perturbations for each  $x$  and retaining that  $\hat{y}_x = \hat{y}_{x'}$  according to their distance to  $x$  [36], ensuring a neighborhood holding a minimum set of samples.

RIS and ROS handle values close to zero in normalization processes. Both large negative and positive values indicate high importance – the sign indicates the direction of the feature’s contribution to the prediction. Therefore, we designed a double-sided clipping method that preserves significant values, either positive or negative, while discarding only those close to zero. In addition, we extended RIS and ROS to provide mean stability values.

To complement our stability evaluation, we introduce the *Run Explanation Stability* (RES) metric to quantify the stability of local explainers across multiple runs on non-perturbed inputs. The core idea behind RES is straightforward: Under fixed model and explanation method settings, the same original input should yield identical explanations [33]. In practice, we generate  $n$  explanations,  $e_{x1}, \dots, e_{xn}$ , for the same original instance  $x$  and compute their standard deviation, returning the maximum deviation in a set of instances. The RES metric is defined as follows:

$$\text{RES}(e_x, \bar{e}_x) = \max_{k=1}^n \|\bar{e}_x - e_{xk}\|, \quad \forall x \in \mathbf{X}. \quad (13)$$

Although we introduce RES as part of the T-Explainer framework, the theoretical foundation behind it came from the Reiteration Similarity metric [5]; however, we simplified the formulation by using the standard deviation as the similarity measure.

RIS, ROS, and RES metrics are unitless quantifiers with no “ideal” desirable values. Reasonable values depend on the context of the application, meaning those metrics must be interpreted relatively by comparing their results across XAI methods [4]. However, lower values indicate methods with higher stability rates. Therefore, RIS and ROS fit into the *stability for slight variations* strategy of the *continuity* category of XAI assessment, while RES fits in the *consistency* category [33].

A faithfulness metric evaluates the extent to which an explanation is faithful to the predictive model it explains. In this sense, we implemented the *Prediction Gap on Important Features* (PGI) [14, 35] metric to evaluate the methods’ faithfulness under the *single/incremental deletion* strategy for *correctness* [33]. Given  $\text{top}(k, e_{\mathbf{x}})$  being the  $k$  most important features determined by a local explanation  $e_{\mathbf{x}}$ , we implemented PGI iterating on  $m$  input instances as follows:

$$\text{PGI}(\mathbf{x}, f, e_{\mathbf{x}}) = \frac{1}{m} \sum_{j=1}^m [||f(\mathbf{x}) - f(\tilde{\mathbf{x}}_j)||] \quad (14)$$

where  $\tilde{x}_i = 0$  [ $i \in \text{top}(k, e_{\mathbf{x}})$ ] and  $f$  return predicted probabilities. PGI values will be in the  $[0, 1]$  interval; the higher the value, the more faithful the explanations are compared to the “true” black-box behavior, as perturbing those  $k$  features caused a significant change in prediction.

Unlike previous implementations, we developed metrics to run all the explainers under evaluation in the same execution cycles. It is an advantage regarding fair comparisons since it ensures the explainers are exposed to the same conditions. Our evaluations are based on automated quantitative metrics, enabling users to formally compare the performances of state-of-the-art feature importance methods. The selected metrics evaluate the consistency, continuity, and correctness dimensions of XAI evaluation [33], providing robust experimental results beyond the typical evaluations in the XAI literature.

## 5 Experiments

This section presents the configurations and outcomes of the experiments undertaken to evaluate T-Explainer, employing a diverse set of datasets, models, and comparison metrics. In all experiments described below, we are evaluating local explanation tasks.

### 5.1 Experimental Setup

We trained Neural Networks from *scikit-learn* library<sup>2</sup> and Gradient-boosted Tree Ensembles from the *XGBoost* library<sup>3</sup> as the black-box models used throughout the experiments. Logistic Regressions and SVMs could also be viable alternatives, but we focused on Neural Networks and Random Forests due to their wide adoption in Machine Learning. The models were trained with a dataset split of 80% for training and 20% for testing. Such division was achieved using the *train\_test\_split* method from *scikit-learn*, with a consistent shuffling seed across all datasets. We conducted a Grid Search to determine the hyperparameters that optimize the models’ performance.

For the Neural Networks, we initialized the hyperparameters search using powers of 2 for the number of neurons in the hidden layers, following standard practices in this context [46].

<sup>2</sup><https://scikit-learn.org/>

<sup>3</sup><https://xgboost.readthedocs.io/>

We employed the ReLU activation function, Stochastic Gradient Descent as the optimizer and the log-loss function. We evaluated alternative activation functions and optimizers, but they did not yield gains. The Tree Ensemble model’s hyperparameters were defined by specifying ranges for the number of decision tree estimators and the maximum depth of each estimator, utilizing cross-entropy loss as the evaluation metric for classification.

We selected three different neural networks from hyperparameter tuning: Three- and five-layer neural networks that hold 64 neuron units per layer (3H-NN and 5H-64-NN, with 9.7K and 18K trainable parameters, respectively) and a five-layer neural network with [64, 128, 128, 128, 64] neurons in each layer (5H-128-NN) and roughly 51K trainable parameters. All neural network models use a learning rate of 0.01, alpha 0.0001, and maximum training epochs of 500. The selected neural networks achieved better performances considering our classification tasks. We based our architectures on previous works [8, 12], with extra neural units and additional layers significantly increasing the training time without noticeably increasing performance.

The Tree Ensemble classifiers (XRFC) have 500 estimators, a maximum depth of 6, a learning rate of 0.01, and a gamma equal to 1. All the other hyperparameters are the libraries’ default for Neural Networks and Tree Ensembles. Those models are used as the base black boxes for comparing the T-Explainer against SHAP [30], LIME [36], and three gradient-based methods from the Captum library [22] – Integrated Gradients, Input  $\times$  Gradient, and DeepLIFT. Specifically, we used the SHAP explainer for neural networks and the TreeSHAP explainer [31] for tree-based classifiers. Although SHAP, LIME, and Gradient-based methods were proposed a few years back, we benchmark T-Explainer with them because they continue to be the most widely used feature attribution explainers in research and practice [3].

For each experiment requiring data perturbation, we used the *NormalPerturbation* method from OpenXAI [3] to generate perturbed neighborhoods with  $\mu = 0$ ,  $\sigma^2 = 0.001$ , a flip percentage  $\varepsilon_p = 0.0001$ , and the perturbation maximum distance of  $h_{\min}/2$ , ensuring neighborhoods with small perturbations around each instance. We also specified the clipping threshold to handle values close to zero as  $\epsilon_c = \pm 10^{-5}$  and the  $l_p$  norm as the Euclidean ( $p = 2$ ).

To improve readability and avoid roundoff issues, we use scientific notation to represent values larger than  $10^5$ , while values smaller than  $10^{-10}$  will be taken as zero.

### 5.2 Synthetic Data

We generate two different synthetic datasets comprising 1,000 instances each. The first is a 4-dimensional (4-FT) dataset where each instance  $\mathbf{x}$  is generated as follows. We distribute the target label  $\mathbf{y} \in [0, 1]$  equally across each dataset half; thus, each class has 500 instances. Conditioned on the value of  $\mathbf{y}$ , we sample the instance  $\mathbf{x}$  as  $x_{1:2} \sim \mathcal{N}(\mu_y, \Sigma_y)$ . We choose  $\mu_0 = [0, 0]^T$  and  $\mu_1 = [-2, 2]^T$ ,

$\Sigma_0 = [[1, 1], [-1, 1]]^T$  and  $\Sigma_1 = \mathbf{I}$ , where  $\mu_0$ ,  $\Sigma_0$  and  $\mu_1$ ,  $\Sigma_1$  denote the means and covariance matrices of the Gaussian distributions associated with instances in classes 0 and 1, respectively. The features  $x_{1:2}$  are called *core\_1* and *core\_2*. Random values are assigned to the features  $x_{3:4}$  (*noise\_1* and *noise\_2*). Such a configuration results in a dataset holding two predictive (important) and two random noise (non-important) features with a small mixture area between the important features to introduce some degree of complexity.

The second synthetic dataset is more robust. It is a 20-dimensional (20-FT) dataset created using the OpenXAI synthetic data generation tool, whose algorithm and properties are described in Agarwal et al. [3]. According to the authors, the algorithm ensures the creation of a dataset that encapsulates feature dependencies and clear local neighborhoods, key properties to guarantee the explanations derived from this synthetic dataset remain consistent with the behavior of the models trained on such data. Using controlled synthetic data for XAI checking meets the correctness dimension of explainability evaluation [33].

We trained the XRFC and 3H-NN models for the synthetic datasets experiments. The XRFC classifier achieved 86.5% accuracy in the 4-FT data and 83.5% accuracy in the 20-FT data, while the 3H-NN model achieved 97.5% accuracy in the 4-FT data and 83.5% accuracy in the 20-FT synthetic dataset. Evaluating explanation methods on accurate models is good practice in controlled settings based on synthetic data [33]. The higher the model’s accuracy level, the more it can be assumed that the model adhered to the reasoning designed in the data.

Note that we are not basing our benchmark experiments on synthetic datasets with massive amounts of instances. We understand that a reasonable amount of data is essential for effectively training and testing machine learning models. According to Aas et al. [1], the well-known feature importance methods become unstable in tasks with more than ten dimensions. In this sense, data dimensionality is more critical to assessing the stability of feature importance methods than the number of instances. Thus, we generate synthetic datasets with enough instances (1,000 for each dataset) to train our models and evaluate XAI methods.

Table 1 shows the stability metrics RIS, ROS, and RES for T-Explainer, TreeSHAP, and LIME, explaining the XRFC model on the 4-FT data. Notice that TreeSHAP has the best RIS, ROS, and RES results. The good performance of TreeSHAP is expected, as 4-FT is a low-dimensional dataset, and TreeSHAP takes advantage of it by relying on a deterministic version of Shapley values computation [5]. Table 2 shows the same metrics for the 3H-NN model in the 4-FT dataset. The T-Explainer performed considerably better than the other XAI methods in RIS ( $7 \times$  better than DeepLIFT), ROS, and the RES metric.

Table 3 presents the PGI results of the explainers applied to the 3H-NN predictions on the 4-FT data. T-Explainer explanations are considerably more faithful than the other methods in identifying the most important feature for predictions (Top

XRFC	RIS		ROS		RES
	XAI	Max	Mean	Max	Mean
T-Exp	13,819	111.4	6e+06	38,904	<b>0</b>
TreeSHAP	<b>5,053</b>	<b>38.0</b>	<b>5e+05</b>	<b>8,226</b>	<b>0</b>
LIME	10,895	200.4	6e+06	86,050	3e-04

**Table 1: Stability of XAI methods explaining the XRFC predictions on the 4-FT synthetic dataset. T-Exp denotes T-Explainer and Max refers to maximum values.**

3H-NN	RIS		ROS		RES
	XAI	Max	Mean	Max	Mean
T-Exp	<b>176</b>	<b>5.97</b>	<b>806</b>	<b>5.82</b>	<b>0</b>
SHAP	2,010	38.59	12,122	51.39	<b>0</b>
LIME	4,625	127.1	1.7e+05	296.9	3e-02
I-Grad	2,465	19.33	1,169	7.41	<b>0</b>
I $\times$ Grad	1,316	9.75	1,535	7.74	1e-05
DeepLIFT	1,316	9.75	1,535	7.74	1e-05

**Table 2: Stability of XAI methods explaining the 3H-NN predictions on the 4-FT dataset. I-Grad and I $\times$ Grad denote Integrated Gradients and Input  $\times$  Gradient, respectively.**

1 column), i.e., T-Explainer’s explanations demonstrated the closest behavior to what the underlying model learned as the most important feature. When the task considered more features, the second and third most important, SHAP outperformed the T-Explainer; however, our method performed consistently more faithfully to the model’s predictions than the other explainers (columns Top 2 and Top 3).

3H-NN	PGI			
	XAI	Top 1	Top 2	Top 3
T-Exp	<b>0.7337</b>	0.7335	0.7334	
SHAP	0.6063	<b>0.8402</b>	<b>0.7569</b>	
LIME	0.4973	0.4960	0.4956	
I-Grad	0.4973	0.4960	0.4956	
I $\times$ Grad	0.4973	0.4960	0.4956	
DeepLIFT	0.4973	0.4960	0.4956	

**Table 3: Faithfulness of XAI methods explaining the 3H-NN predictions on the 4-FT dataset according to the Top  $k$  most important features.**

Tables 4 and 5 represent the stability of the XRFC and 3H-NN models in the 20-FT dataset. In Table 4, we observe that the T-Explainer is superior to TreeSHAP and LIME in the RIS and ROS metrics for both the maximum and mean values. TreeSHAP reached a close performance regarding maximum ROS, but T-Explainer is considerably better in average ROS. Similar results can be observed in Table 5, where the T-Explainer outperforms all other explainers in terms of RIS ( $3 \times$  better than Integrated Gradients), with

slightly better performance than Integrated Gradients in the mean ROS but outperforms the other explainers in maximum ROS.

SHAP was the most unstable method, which can be justified in the context of the 20-FT dataset because, in high-dimensional spaces, SHAP uses a random sampling algorithm rather than a deterministic one, leading to unstable explanations [5]. Moreover, SHAP is also prone to extrapolations [20, 21].

XRFC	RIS		ROS		RES	
	XAI	Max	Mean	Max	Mean	
T-Exp	<b>728</b>	<b>28.95</b>	<b>2.6e+06</b>	<b>35,596</b>	<b>0</b>	
TreeSHAP	897	37.83	3.3e+06	64,204	<b>0</b>	
LIME	1,117	143.6	21.6e+06	3.5e+05	1e-04	

**Table 4: Stability of XAI methods explaining the XRFC predictions on the 20-FT synthetic dataset.**

3H-NN	RIS		ROS		RES	
	XAI	Max	Mean	Max	Mean	
T-Exp	<b>717</b>	<b>26.2</b>	<b>17,887</b>	<b>99.98</b>	<b>0</b>	
SHAP	2.8e+05	7,272	2e+06	14,076	2e-01	
LIME	10,182	125.6	28,063	301.9	3e-02	
I-Grad	2,279	28.35	39,287	107.4	<b>0</b>	
I×Grad	11,815	63.36	60,787	217.2	5e-06	
DeepLIFT	11,813	63.36	60,781	217.2	5e-06	

**Table 5: Stability of XAI methods explaining the 3H-NN predictions on the 20-FT dataset.**

In general, Tables 1, 2, 4, and 5 show that the T-Explainer is robust in different stability metrics that evaluate the consistency and continuity of explanations in controlled synthetic data tasks [33], being among the best performance methods, especially when the data dimensionality is high.

Observing the PGI results in Table 6, we have the T-Explainer as the most faithful explanation method for the predictive behavior of the original model for the most important feature (Top 1 column). Enlarging the set of the most important  $k$  features (Top 3–9 columns), SHAP presented the best performances; however, T-Explainer consistently outperformed all the other explainers, being the second most faithful explanation method explaining the 3H-NN predictions on the 20-FT synthetic dataset.

Figure 2 compares the RIS and ROS metrics. Once they are based on normal perturbations, we executed both metrics multiple times to evaluate the behavior of the XAI explainers and add statistical significance to our empirical experiments. We randomly selected 100 samples from the 20-FT data (fixing the same seed throughout the experiment for reproducibility) and performed RIS and ROS metrics 10 times each, evaluating explanations of the 3H-NN model. Similarly to previous experiments, we present the maximum and mean values of RIS and ROS over the runs. The boxplots in Figure 2 show

XAI	3H-NN				
	Top 1	Top 3	Top 5	Top 7	Top 9
T-Exp	<b>0.5913</b>	0.5738	0.5674	0.5624	0.5669
SHAP	0.5844	<b>0.6540</b>	<b>0.6467</b>	<b>0.6580</b>	<b>0.6724</b>
LIME	0.4586	0.4548	0.4536	0.4536	0.4535
I-Grad	0.4562	0.4540	0.4538	0.4536	0.4536
I×Grad	0.5604	0.5621	0.5501	0.5482	0.5504
DeepLIFT	0.5604	0.5621	0.5501	0.5482	0.5504

**Table 6: Faithfulness of XAI methods explaining the 3H-NN predictions on the 20-FT dataset according to the Top  $k$  most important features.**

that T-Explainer is ranked among the most stable approaches, following the earlier findings presented in Table 5.

In summary, T-Explainer’s performance when dealing with the XRFC classifier, a non-differentiable model, was remarkable for more complex tasks (e.g., explaining predictions for the 20-FT data). Such performances have significant practical implications, suggesting that the T-Explainer might perform well even when applied to generate explanations for non-differentiable machine learning models. The following section presents the evaluation results on real-world data.

### 5.3 Real-world Data

This Section extends the evaluations and comparisons by applying real-world data from different domains. Specifically, we run experiments using four well-known real-world datasets with distinct properties regarding dimensionality, the presence of categorical attributes, and size.

The Banknote Authentication [29] is a 4-dimensional dataset containing 1,372 instances with measurements of genuine and forged banknote specimens. The German Credit [19] comprises 9 features (numerical and categorical) covering financial, demographic, and personal information from 1,000 credit applicants, each categorized into good or bad risk.

The Home Equity Line of Credit (HELOC) dataset provided by FICO [17] consists of financial attributes from anonymized applications for home equity lines of credit submitted by 9,871 real homeowners. The task in the HELOC dataset is to predict whether an applicant has a good or bad risk of repaying the HELOC account within two years. The largest dataset in our study is HIGGS [8], which contains 28 features about simulated collision events to distinguish between Higgs bosons signals and a background process. The original HIGGS dataset contains 11 million instances, but we used the 98,050 instances version available at OpenML [49]. Table 7 summarizes the real datasets.

The experiments with real-world data were conducted using only the neural network models, as some of the explanation models with which T-Explainer is compared are specifically designed for neural networks. Moreover, the neural network models are differentiable, thus meeting the theoretical require-

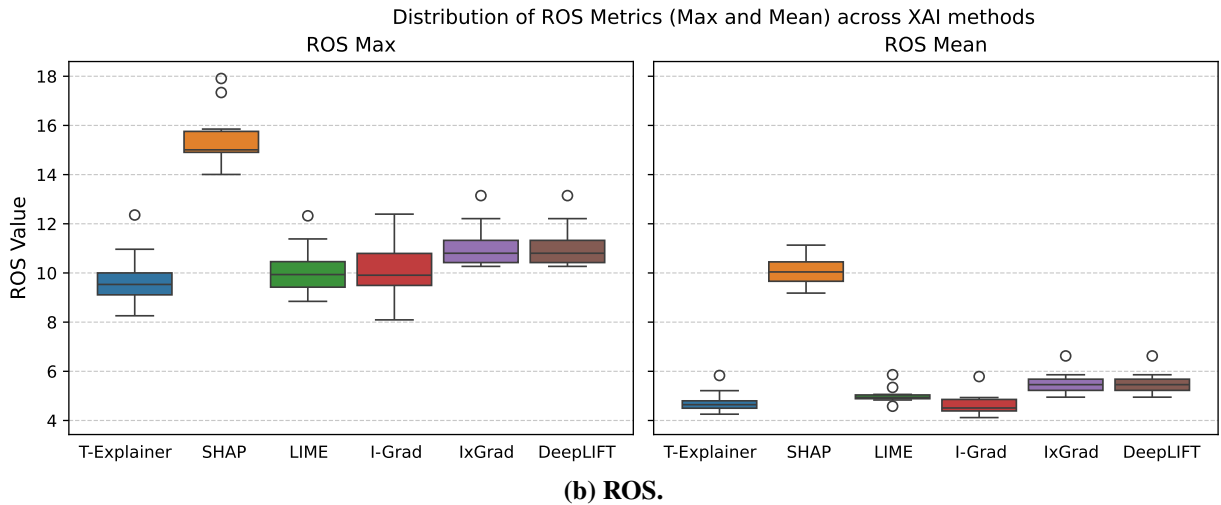
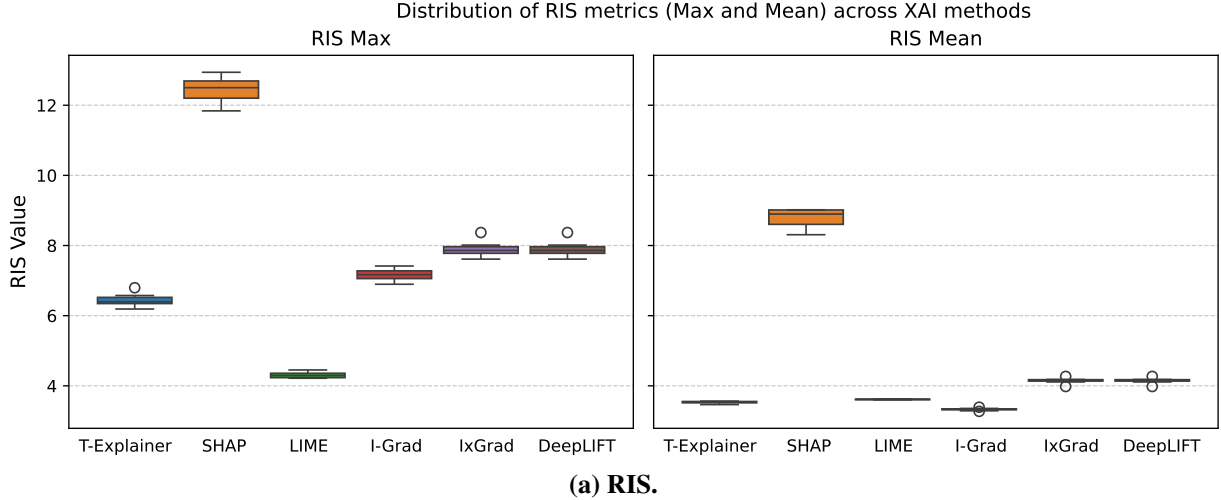


**Figure 2: Behavior of XAI methods explaining samples predicted with the 3H-NN model trained on the 20-FT dataset when running RIS and ROS metrics multiple times. The y-axes are on a logarithmic scale for better visualization.**

	Banknote	German	HELOC	HIGGS
#Instances	1,372	1,000	9,871	98,050
#Num features	4	4	21	28
#Cat features	0	5	2	0
#Classes	2	2	2	2

**Table 7: Properties of the real datasets. Num features and Cat features refer to numeric and categorical features, respectively.**

ments that support the T-Explainer technique. We further discuss tree-based models in Section 7.

For experiments with Banknote Authentication and German Credit datasets, we selected the 3H-NN model. In Table 8, one can see that T-Explainer is less stable than Integrated

Gradients, but it is the second-best method on average for RIS and ROS (tied with Integrated Gradients for RES).

3H-NN	RIS		ROS		RES	
	XAI	Max	Mean	Max	Mean	Max
T-Exp		175.29	3.09	429.31	4.05	<b>0</b>
SHAP		1.3e+05	468	1.9e+05	543	<b>0</b>
LIME		97.57	9.34	849.02	13.43	3e-02
I-Grad		<b>12.37</b>	<b>1.54</b>	429.23	<b>2.09</b>	<b>0</b>
I $\times$ Grad		175.33	4.41	<b>427.97</b>	4.12	2e-05
DeepLIFT		175.33	4.41	<b>427.97</b>	4.12	2e-05

**Table 8: Stability of XAI methods explaining the 3H-NN predictions on the Banknote Authentication dataset.**

Analyzing the PGI results in Table 9, we see that all the methods are tied to a faithful behavior between explanations and model predictions according to the most important feature

identified in their explanations. However, T-Explainer's performance grows when considering the second and third most important features. Only SHAP and T-Explainer achieved a faithfulness higher than 0.5 for their explanations' three most important features. In a low-dimensional (four features, see Table 7) set such as the Banknote Authentication, it is possible to conjecture that an explainer with a PGI below 0.5 generally lacks a highly significant feature in its explanations.

3H-NN		PGI		
XAI		Top 1	Top 2	Top 3
T-Exp	0.4514	<b>0.7304</b>	<b>0.9563</b>	
SHAP	0.4514	0.4514	0.4464	
LIME	0.4514	0.4514	0.6634	
I-Grad	0.4514	0.4514	0.4514	
I $\times$ Grad	0.4514	0.4514	0.4514	
DeepLIFT	0.4514	0.4514	0.4514	

**Table 9: Faithfulness of XAI methods explaining the 3H-NN predictions on the Banknote Authentication dataset according to the Top  $k$  most important features.**

Table 10 presents the stability tests for the predictions of the 3H-NN model on the German Credit data. The original version of the dataset has 20 numerical and categorical attributes. However, applying it directly to a machine learning task is difficult due to its intricate categorization system. We pre-processed the German Credit data to clean it, resulting in a reduced version holding nine features (4 numerical and 5 categorical features, see Table 7). As shown in Table 10, the T-Explainer performed as the most stable explainer regarding RIS and maximum ROS perturbations, being the second best for the mean ROS.

XAI	RIS		ROS		RES
	Max	Mean	Max	Mean	Max
T-Exp	<b>1,971</b>	<b>49.4</b>	<b>15,735</b>	239.9	<b>0</b>
SHAP	1.0e+06	14,044	2.5e+07	62,883	2.1e-01
LIME	7,547	131.1	1.8e+05	739.9	2.4e-02
I-Grad	8,709	59.5	58,721	<b>185.7</b>	<b>0</b>
I $\times$ Grad	10,933	63.2	1.0e+05	350.8	2.8e-06
DeepLIFT	10,934	63.2	1.0e+05	350.8	2.4e-06

**Table 10: Stability of XAI methods explaining the 3H-NN predictions on the German Credit dataset.**

Table 11 shows close performances regarding the PGI metric among all feature importance methods for 3H-NN predictions on German Credit data. LIME, the T-Explainer, and SHAP were the most faithful explainers in the incremental verification process of the top  $k$  features.

Tables 8 and 10 indicate that gradient-based methods are more stable to input/output perturbations than SHAP and, in some cases, also than LIME. As one can notice, the T-Explainer competes quite well with other gradient-based methods regarding stable explanations. Although Tables 9 and 11 place

XAI	PGI				
	Top 1	Top 3	Top 5	Top 7	Top 9
T-Exp	0.8044	0.8164	<b>0.8311</b>	0.8198	0.8178
SHAP	0.8245	0.8193	0.8215	<b>0.8242</b>	<b>0.8240</b>
LIME	<b>0.8396</b>	<b>0.8231</b>	0.8196	0.8184	0.8187
I-Grad	0.8257	0.8182	0.8156	0.8159	0.8159
I $\times$ Grad	0.8149	0.8212	0.8222	0.8220	0.8220
DeepLIFT	0.8149	0.8212	0.8222	0.8220	0.8220

**Table 11: Faithfulness of XAI methods explaining the 3H-NN predictions on the German Credit dataset according to the Top  $k$  most important features.**

the T-Explainer between the better feature importance methods for faithful explanations.

HELOC and HIGGS are more robust datasets in terms of dimensionality and size. We selected the 3H-NN and the five-layer neural network models to compare T-Explainer with the other explainers on the real-world datasets. Specifically, we trained the 3H-NN and 5H-128-NN classifiers in HELOC, achieving 71.34% and 73.27% of accuracy, respectively. Despite the accuracy values being lower than those we achieved before, these performances align with the results reported in the literature [12].

Table 12 shows that Integrated Gradients is the most stable explainer for almost all metrics (behind LIME only for mean RIS but with very close numbers). However, we highlight the performance of T-Explainer, especially regarding the metrics' means. Only Integrated Gradients, LIME, and T-Explainer kept the mean RIS under ten units, which can be taken as virtually the same mean stability to input perturbations. Similar results are observed in mean ROS, where Integrated Gradients, LIME, and T-Explainer achieved the smallest values, with T-Explainer the second best. Table 13 shows the stability of the explainers when applied to the five-layer neural network. T-Explainer was the most stable method, with Integrated Gradients being the second best for mean RIS and LIME as the second best for mean ROS. Only the T-Explainer and Integrated Gradients achieved the highest levels of stability in RES.

XAI	RIS		ROS		RES
	Max	Mean	Max	Mean	Max
T-Exp	1,443	8.49	94,943	527.9	<b>0</b>
SHAP	84,794	1,330	1.7e+07	64,693	1.5e-02
LIME	509.7	<b>3.84</b>	3.7e+05	626.5	9.3e-02
I-Grad	<b>159.8</b>	4.21	<b>85,463</b>	<b>401.1</b>	<b>0</b>
I $\times$ Grad	3,754	33.67	3.5e+05	1,879	8.7e-07
DeepLIFT	3,749	33.64	3.5e+05	1,878	9.0e-07

**Table 12: Stability of XAI methods explaining the 3H-NN predictions on the HELOC dataset.**

5H-128-NN		RIS		ROS		RES
XAI		Max	Mean	Max	Mean	Max
T-Exp	<b>154.0</b>	<b>5.37</b>	<b>1.4e+05</b>	<b>362.5</b>	<b>0</b>	
SHAP	52,924	1,757	1.6e+07	67,451	1.9e-01	
LIME	5,083	39.96	2.5e+05	935.0	1.6e-02	
I-Grad	255.7	7.21	1.9e+07	19,283	<b>0</b>	
I $\times$ Grad	11,769	66.01	4.3e+05	3,215	1.8e-06	
DeepLIFT	11,785	66.06	4.3e+05	3,218	1.7e-06	

**Table 13: Stability of XAI methods explaining the 5H-128-NN predictions on the HELOC dataset.**

Tables 14 and 15 present the PGI performance of the explainers. All methods increased their faithfulness values by including more features in the set of top  $k$  features, indicating that the HELOC dataset has multiple significant features for the underlying model. For the 3H-NN model, the T-Explainer presented the highest PGI value considering the nine most essential features, i.e., our method could identify nine important features with high fidelity to the predictions of the model out of more than 20 predictive features. For the 5H-128-NN model, T-Explainer performed better up to the three most essential features, although our method was the second with higher PGI, after Integrated Gradients, the most faithful explainer to larger top  $k$  feature sets.

3H-NN		PGI				
XAI		Top 1	Top 3	Top 5	Top 7	Top 9
T-Exp	0.6360	0.7364	0.8146	0.8595	<b>0.8712</b>	
SHAP	0.6309	0.6529	0.7268	0.7740	0.7995	
LIME	0.6274	0.6543	0.8350	0.8424	0.8449	
I-Grad	<b>0.6379</b>	<b>0.7774</b>	<b>0.8557</b>	<b>0.8614</b>	0.8622	
I $\times$ Grad	<b>0.6379</b>	0.7710	0.8436	0.8539	0.8419	
DeepLIFT	<b>0.6379</b>	0.7710	0.8436	0.8539	0.8419	

**Table 14: Faithfulness of XAI methods explaining the 3H-NN predictions on the HELOC dataset according to the Top  $k$  most important features.**

5H-128-NN		PGI				
XAI		Top 1	Top 3	Top 5	Top 7	Top 9
T-Exp	<b>0.7028</b>	<b>0.7454</b>	0.7470	0.7689	0.7821	
SHAP	0.6373	0.6617	0.6948	0.7329	0.7667	
LIME	0.6627	0.7044	<b>0.8022</b>	0.7223	0.7663	
I-Grad	0.6763	0.7130	0.7617	<b>0.7923</b>	<b>0.7910</b>	
I $\times$ Grad	0.6506	0.6847	0.7198	0.7445	0.7566	
DeepLIFT	0.6506	0.6847	0.7198	0.7445	0.7566	

**Table 15: Faithfulness of XAI methods explaining the 5H-128-NN predictions on the HELOC dataset according to the Top  $k$  most important features.**

We trained the 3H-NN and 5H-64-NN classifiers on HIGGS data, which achieved accuracy 69.58% and 66.83%, respectively, close to the values reported in previous work [12]. We included a set of benchmarks using a five-layer neural network here to maintain some similarity to the architectures proposed in Baldi et al. [8], which explored the use of deep networks in HIGGS. Tables 16 and 17 show good stability performances of gradient-based feature importance explainers. T-Explainer outperforms them in RIS perturbations and remains competitive in ROS and RES metrics. Such results demonstrate the ability of the T-Explainer to generate consistent explanations through different levels of model complexity and data dimensionality. Note that SHAP is more unstable than LIME, with SHAP's claimed advantageous performance predominantly seen in low-dimensional datasets [5].

Tables 14 and 15 present the PGI performance of the explainers. All methods increased their faithfulness values by including more features in the set of top  $k$  features, indicating that the HELOC dataset has multiple significant features for the underlying model. For the 3H-NN model, the T-Explainer presented the highest PGI value considering the nine most essential features, i.e., our method could identify nine important features with high fidelity to the predictions of the model out of more than 20 predictive features. For the 5H-128-NN model, T-Explainer performed better up to the three most essential features, although our method was the second with higher PGI, after Integrated Gradients, the most faithful explainer to larger top  $k$  feature sets.

3H-NN		RIS		ROS		RES
XAI		Max	Mean	Max	Mean	Max
T-Exp	<b>1,063</b>	<b>45.0</b>	69,645	304.4	<b>0</b>	
SHAP	1.4e+05	5,213	8.8e+05	22,190	2.05e-01	
LIME	4,424	90.0	69,458	492.6	3.19e-02	
I-Grad	3,833	49.7	<b>27,719</b>	<b>272.4</b>	<b>0</b>	
I $\times$ Grad	2,030	79.9	70,159	604.3	6.62e-06	
DeepLIFT	2,031	79.9	70,153	604.3	6.32e-06	

**Table 16: Stability of XAI methods explaining the 3H-NN predictions on the HIGGS dataset.**

5H-64-NN		RIS		ROS		RES
XAI		Max	Mean	Max	Mean	Max
T-Exp	<b>1,359</b>	<b>57.7</b>	65,999	<b>330.4</b>	<b>0</b>	
SHAP	1.3e+05	4,309	7.3e+06	19,999	2.22e-01	
LIME	9,582	130.8	46,700	477.2	3.50e-02	
I-Grad	15,619	101.1	<b>37,091</b>	452.2	<b>0</b>	
I $\times$ Grad	4,036	123.9	84,022	558.6	1.67e-05	
DeepLIFT	4,036	123.9	84,021	558.6	1.69e-05	

**Table 17: Stability of XAI methods explaining the 5H-64-NN predictions on the HIGGS dataset.**

Tables 18 and 19 present the PGI performance of the explainers in the HIGGS dataset. LIME achieved the highest PGI values when explaining predictions made by the 3H-NN and 5H-64-NN neural networks. However, T-Explainer is the second best in describing faithful explanations when considering larger top  $k$  feature sets (see Top 7 and 9 columns).

Finally, the experiments above show that T-Explainer generally performs well, clearly outperforming well-known model-agnostic methods such as SHAP (and LIME for most tests). Moreover, T-Explainer also proved quite competitive with model-specific techniques such as gradient-based ones, thus becoming a new and valuable alternative method for explaining black-box models' predictions.

3H-NN		PGI				
XAI		Top 1	Top 3	Top 5	Top 7	Top 9
T-Exp		0.6322	0.6291	0.6395	0.6297	0.6414
SHAP		0.6355	0.6111	0.6007	0.5920	0.5955
LIME		<b>0.7155</b>	<b>0.7075</b>	<b>0.6841</b>	<b>0.6877</b>	<b>0.6827</b>
I-Grad		0.6380	0.5921	0.5935	0.6071	0.6073
I $\times$ Grad		0.6704	0.6367	0.6236	0.6231	0.6351
DeepLIFT		0.6704	0.6367	0.6236	0.6231	0.6351

**Table 18: Faithfulness of XAI methods explaining the 3H-NN predictions on the HIGGS dataset according to the Top  $k$  most important features.**

5H-64-NN		PGI				
XAI		Top 1	Top 3	Top 5	Top 7	Top 9
T-Exp		0.6094	0.5923	0.6043	0.6335	0.6357
SHAP		0.5664	0.5838	0.5941	0.6029	0.6292
LIME		<b>0.6768</b>	<b>0.6769</b>	<b>0.6724</b>	<b>0.6545</b>	<b>0.6510</b>
I-Grad		0.6441	0.6074	0.5897	0.5833	0.5916
I $\times$ Grad		0.6221	0.6109	0.6074	0.6228	0.6215
DeepLIFT		0.6221	0.6109	0.6074	0.6228	0.6215

**Table 19: Faithfulness of XAI methods explaining the 5H-64-NN predictions on the HIGGS dataset according to the Top  $k$  most important features.**

## 6 Computational Performance

Another challenge that XAI methods have to face is related to computational performance. Shapley-based approaches like SHAP apply sampling approximations because the exact version of the method is an NP-hard problem with exponential computing time regarding the number of features [30]. SHAP is a leading method in feature attribution tasks due to its axiomatic properties, with a range of explainers based on different algorithms, from the exact version to optimized approaches. However, according to its documentation, the most precise algorithm is only feasible for modelings that are nearly limited to 15 features<sup>4</sup>.

For a computational comparison of the performance of the T-Explainer, we generated a synthetic dataset with 16 features (16-FT) using OpenXAI, similar to the 20-FT dataset we used before (see the Synthetic Data Section). The 3H-NN model was trained with the 16-FT dataset according to the experimental setup defined in Section 5.1. We then defined ten explanation tasks, increasing the number of explanations by ten instances from the 16-FT data for each task, ranging from ten to one hundred explanations, to compare the T-Explainer with three implementations of SHAP – the optimized explainer (the same method used in the stability experiments of Section 5), KernelSHAP [30], the exact explainer based on standard Shapley values computation. Figure 3 presents the computational performance of T-Explainer and SHAP. The

*y*-axis (time) of Figure 3 is on a logarithmic scale for better visualization purposes.

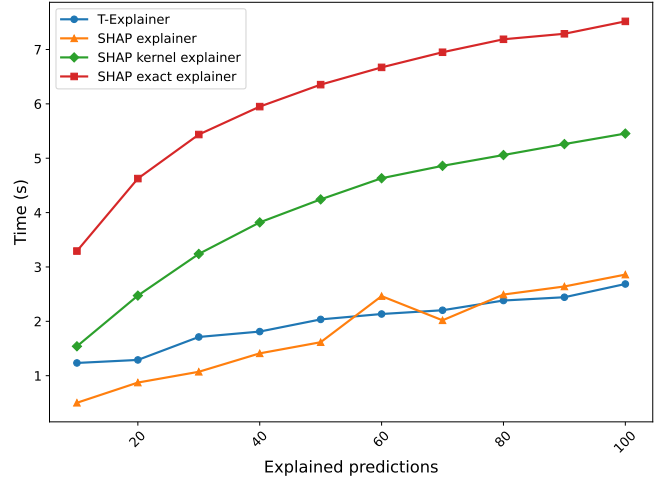


**Figure 3: Running times (in log scale) of T-Explainer and SHAP explainers applied to the 3H-NN model trained on 16-dimensional synthetic data.**

SHAP explainer was the fastest for the first five iterations (explaining sets with 10 to 50 instances). However, the method was the most unstable, as we demonstrated in the stability evaluations. However, the performance of the T-Explainer is quite close to that of the SHAP explainer, and it performs faster than it for sets with 80 instances and above. KernelSHAP was slightly more expensive for small sets of instances, while the SHAP exact explainer running time has grown exponentially. In such a performance test, we used a reduced dataset instead of the 20-FT data because applying the SHAP exact explainer in tasks with more than 16 features is currently impossible. Most machine learning problems involve high-dimensional data. For example, HIGGS is a 28-dimensional dataset with over 98 thousand instances. With that dataset, it is impossible to apply the exact version of SHAP, and the optimized version of SHAP performs very poorly. Something similar could be said about the HELOC data, which recently motivated a challenge by FICO [17]. In this sense, T-Explainer is placed as a highly competitive XAI approach regarding computational resources.

## 7 Discussion, Limitations, and Future Work

T-Explainer is backed by a clearly defined deterministic optimization process for calculating partial derivatives. This new approach gives T-Explainer more robustness, as demonstrated in our results.

Our experiments have focused on binary classification models, which are known to perform well in supervised learning [12]. However, there is no constraint in applying T-Explainer to regression problems or more complex models, such as deep learning models. The T-Explainer naturally supports regression or multiclass classification with minor adaptations, which we are currently working on.

<sup>4</sup><https://shap.readthedocs.io/ExactExplainer>, visited in July 2024

Although T-Explainer has demonstrated competitive results when applied to tree-based models on synthetic data, tree-based architectures impose extra challenges on XAI. Tree classifiers have non-continuous architectures in which constant values are stored in leaf nodes, rendering gradient-based methods inappropriate. The current version of T-Explainer is not yet fully developed to support tree-based models. We are currently designing a mechanism that enables the computation of gradients in tree-based models, extending T-Explainer to operate in a more general context.

The present implementation of the T-Explainer can handle categorical attributes. It uses an approach that discretizes categorical data into intervals using continuous perturbations, enabling the computation of partial derivatives. However, the approach requires a model retraining to fit the continuous intervals induced in the columns containing one-hot encoded categorical attributes. Retraining introduces additional computational complexity. Getting around the retraining issue is another improvement that we are currently working on. An alternative approach we are considering in this context is to apply the target encoding transformer [9], which converts each nominal value of a categorical attribute into its corresponding expected value.

Another aspect under improvement is the  $\mathbf{h}$  optimization module. To our knowledge, there is no closed solution to determine an optimum value of  $\mathbf{h}$  in this context. During our investigations, we observed that the finite difference computation presents a certain instability for instances near the model’s decision boundaries due to discontinuities imposed by the decision boundaries. The literature on numerical methods offers many alternatives to deal with discontinuities when approximating derivatives through finite differences [38, 47]. We refer to methods that develop Generalized Finite Differences (GFD) among the alternative approaches [10, 43]. As part of the T-Explainer’s core, we are investigating alternatives to refine the  $\mathbf{h}$  optimization process while maintaining computational efficiency.

We conducted experiments and comparisons using tabular data to create classification models for simplicity and because it is a typical setup for machine learning problems in academia and industry [12]. We highlight that our experimental setup followed the evaluation practices in the recent literature [8, 46], focusing on Neural Networks as black boxes and including datasets where leading XAI approaches have stability and applicability difficulties. However, we designed the T-Explainer considering more complex data representations, such as 2D images, videos, or semantic segmentation. We are extending our approach to include simplification masking approaches, a strategy widely used by many XAI methods [30, 36].

The T-Explainer framework provides other metrics to evaluate feature importance in addition to those included in this publication, released as a Python module. We are actively extending this module to encompass more metrics and ensure their robustness, efficiency, and flexibility. A comprehensive evaluation of an explanation method requires quantitative [11] and qualitative [50] assessments. We prioritized quantitative

metrics in this work, particularly those for evaluating consistency, continuity, and correctness [33]. We are committed to comprehensively validating the T-Explainer using metrics beyond those discussed here.

When carefully developed and applied, explainability contributes by adding new trustworthy perspectives to the broad horizon of Machine Learning, enriching the next generation of transparent Artificial Intelligence applications [26]. As an evolving project, T-Explainer will continue to be expanded and updated, incorporating additional functionalities and refinements. Our goal is to provide a complete XAI suite in Python based on implementations of T-Explainer and its functionalities in a well-documented and user-friendly package.

## 8 Conclusion

In this paper, we present the T-Explainer, a Taylor expansion-based XAI technique. It is a deterministic local feature attribution method built on a solid mathematical foundation that grants it relevant properties. Moreover, T-Explainer is designed to be a model-agnostic method capable of generating explanations for a wide range of machine learning models, as it relies only on the models’ outputs without accounting for their internal structure or partial results. The experiments and comparisons demonstrate that the T-Explainer is stable and accurate compared to model-specific techniques, thus making it a valuable explanation alternative.

## Acknowledgments

This work was partially supported by the Coordenação de Aperfeiçoamento de Pessoal de Nível Superior–Brasil (CAPES)–Finance Code 001, by CNPq Grant 307184/2021-8, and by the São Paulo Research Foundation (FAPESP) Grant 2022/09091-8. The views expressed in this material are the authors’ responsibility and do not necessarily reflect the views of the funding agencies.

## References

- [1] Kjersti Aas, Martin Jullum, and Anders Løland. Explaining individual predictions when features are dependent: More accurate approximations to shapley values. *Artificial Intelligence*, 298:103502, 2021.
- [2] Amina Adadi and Mohammed Berrada. Peeking inside the black-box: A survey on explainable artificial intelligence (XAI). *IEEE Access*, 6:52138–52160, 2018.
- [3] Chirag Agarwal, Satyapriya Krishna, Eshika Saxena, Martin Pawelczyk, Nari Johnson, Isha Puri, Marinka Zitnik, and Himabindu Lakkaraju. OpenXAI: Towards a transparent evaluation of model explanations. In *Advances in Neural Information Processing Systems*, volume 35, pages 15784–15799. Curran Associates, Inc., 2022.
- [4] David Alvarez-Melis and Tommi S Jaakkola. Towards robust interpretability with self-explaining neural networks. *Advances in Neural Information Processing Systems*, 31, 2018.

[5] Elvio Amparore, Alan Perotti, and Paolo Bajardi. To trust or not to trust an explanation: Using LEAF to evaluate local linear XAI methods. *PeerJ Computer Science*, 7:e479, 2021.

[6] Alejandro Barredo Arrieta, Natalia Díaz-Rodríguez, Javier Del Ser, Adrien Bennetot, Siham Tabik, Alberto Barbado, Salvador García, Sergio Gil-López, Daniel Molina, Richard Benjamins, et al. Explainable artificial intelligence (XAI): Concepts, taxonomies, opportunities and challenges toward responsible AI. *Information Fusion*, 58:82–115, 2020.

[7] Sebastian Bach, Alexander Binder, Grégoire Montavon, Frederick Klauschen, Klaus-Robert Müller, and Wojciech Samek. On pixel-wise explanations for non-linear classifier decisions by layer-wise relevance propagation. *PLOS One*, 10(7):e0130140, 2015.

[8] Pierre Baldi, Peter Sadowski, and Daniel Whiteson. Searching for exotic particles in high-energy physics with deep learning. *Nature Communications*, 5(1):4308, 2014.

[9] Konrad Banachewicz, Luca Massaron, and Anthony Goldbloom. *The Kaggle Book: Data analysis and machine learning for competitive data science*. Packt Publishing Ltd, Birmingham, UK, 2022.

[10] JJ Benito, F Urena, L Gavete, and R Alvarez. An h-adaptive method in the generalized finite differences. *Computer Methods in Applied Mechanics and Engineering*, 192(5-6):735–759, 2003.

[11] Francesco Bodria, Fosca Giannotti, Riccardo Guidotti, Francesca Naretto, Dino Pedreschi, and Salvatore Rinzivillo. Benchmarking and survey of explanation methods for black box models. *Preprint arXiv:2102.13076*, 2021.

[12] Vadim Borisov, Tobias Leemann, Kathrin Seßler, Johannes Haug, Martin Pawelczyk, and Gjergji Kasneci. Deep neural networks and tabular data: A survey. *IEEE Transactions on Neural Networks and Learning Systems*, 7:1–41, 2022.

[13] Leo Breiman. Random forests. *Machine Learning*, 45(1):5–32, 2001.

[14] Jessica Dai, Sohini Upadhyay, Ulrich Aivodji, Stephen H Bach, and Himabindu Lakkaraju. Fairness via explanation quality: Evaluating disparities in the quality of post hoc explanations. In *AAAI/ACM Conference on AI, Ethics, and Society*, pages 203–214, 2022.

[15] Jamie Duell, Xiuyi Fan, Bruce Burnett, Gert Aarts, and Shang-Ming Zhou. A comparison of explanations given by explainable artificial intelligence methods on analysing electronic health records. In *IEEE EMBS Int. Conf. on Biomedical and Health Informatics*, pages 1–4. IEEE, 2021.

[16] EU Regulation. 2016/679 of the European Parliament and of the council of 27 april 2016 on the General Data Protection Regulation. <http://data.europa.eu/eli/reg/2016/679/oj>, 2016. Online, visited on April 2023.

[17] FICO. Home equity line of credit (HELOC) dataset. <https://community.fico.com/s/explainable-machine-learning-challenge>, 2019. Accessed: 2023-09-10.

[18] Alex Gramagna and Paolo Giudici. SHAP and LIME: An evaluation of discriminative power in credit risk. *Frontiers in Artificial Intelligence*, 4:752558, 2021.

[19] Hans Hofmann. Statlog (German Credit Data). UCI Repository. Irvine: University of California, School of Information and Computer Sciences, 1994.

[20] Giles Hooker and Lucas Mentch. Please stop permuting features: An explanation and alternatives. *Preprint arXiv:1905.03151*, 2019.

[21] Giles Hooker, Lucas Mentch, and Siyu Zhou. Unrestricted permutation forces extrapolation: Variable importance requires at least one more model, or there is no free variable importance. *Statistics and Computing*, 31(6):1–16, 2021.

[22] Narine Kokhlikyan, Vivek Miglani, Miguel Martin, Edward Wang, Bilal Alsallakh, Jonathan Reynolds, Alexander Melnikov, Natalia Kliushkina, Carlos Araya, Siqi Yan, et al. Captum: A unified and generic model interpretability library for PyTorch. *Preprint arXiv:2009.07896*, 2020.

[23] Satyapriya Krishna, Tessa Han, Alex Gu, Javin Pombra, Shahin Jabbari, Steven Wu, and Himabindu Lakkaraju. The disagreement problem in explainable machine learning: A practitioner’s perspective. *Preprint arXiv:2202.01602*, 2022.

[24] Murat Kuzlu, Umit Cali, Vinayak Sharma, and Özgür Güler. Gaining insight into solar photovoltaic power generation forecasting utilizing explainable artificial intelligence tools. *IEEE Access*, 8:187814–187823, 2020.

[25] Himabindu Lakkaraju, Nino Arsov, and Osbert Bastani. Robust and stable black box explanations. In *International Conference on Machine Learning*, pages 5628–5638. PMLR, 2020.

[26] Sebastian Lapuschkin, Stephan Wäldchen, Alexander Binder, Grégoire Montavon, Wojciech Samek, and Klaus-Robert Müller. Unmasking Clever Hans predictors and assessing what machines really learn. *Nature Communications*, 10(1):1–8, 2019.

[27] Randall J LeVeque. *Finite difference methods for ordinary and partial differential equations: steady-state and time-dependent problems*. SIAM, Philadelphia, PA, USA, 2007.

[28] Pantelis Linardatos, Vasilis Papastefanopoulos, and Sotiris Kotsiantis. Explainable ai: A review of machine learning interpretability methods. *Entropy*, 23(1):18, 2020.

[29] Volker Lohweg. Banknote Authentication. UCI Repository. Irvine: University of California, School of Information and Computer Sciences, 2013.

[30] Scott M Lundberg and Su-In Lee. A unified approach to interpreting model predictions. In *Advances in Neural Information Processing Systems*, volume 30, pages 4768–4777, Long Beach, CA, USA, 2017. Curran Associates Inc.

[31] Scott M Lundberg, Gabriel G Erion, and Su-In Lee. Consistent individualized feature attribution for tree ensembles. *Preprint arXiv:1802.03888*, 2018.

[32] Jerrold E Marsden and Anthony Tromba. *Vector calculus*. Macmillan, United Kingdom, 2011.

[33] Meike Nauta, Jan Trienes, Shreyasi Pathak, Elisa Nguyen, Michelle Peters, Yasmin Schmitt, Jörg Schlöterer, Maurice van Keulen, and Christin Seifert. From anecdotal evidence to quantitative evaluation methods: A systematic review on evaluating explainable AI. *ACM Computing Surveys*, 55(13s), 2023.

[34] Evandro S Ortigossa, Thales Gonçalves, and Luis Gustavo Nonato. Explainable artificial intelligence (XAI)–From theory to methods and applications. *IEEE Access*, 12:80799–80846, 2024.

[35] Vitali Petsiuk, Abir Das, and Kate Saenko. RISE: Randomized input sampling for explanation of black-box models. *Preprint arXiv:1806.07421*, 2018.

[36] Marco Tulio Ribeiro, Sameer Singh, and Carlos Guestrin. “Why should I trust you?” Explaining the predictions of any classifier. In *Proceedings of the 22nd ACM SIGKDD International Conference on Knowledge Discovery and Data Mining*, pages 1135–1144, San Francisco, CA, USA, 2016. NY ACM.

[37] Pau Rodríguez, Miguel A. Bautista, Jordi González, and Sergio Escalera. Beyond one-hot encoding: Lower dimensional target embedding. *Image and Vision Computing*, 75:21–31, 2018.

[38] Katya Scheinberg. Finite difference gradient approximation: To randomize or not? *INFORMS Journal on Computing*, 34(5):2384–2388, 2022.

[39] Avanti Shrikumar, Peyton Greenside, and Anshul Kundaje. Learning important features through propagating activation differences. In *34th International Conference on Machine Learning*, pages 3145–3153, Sydney, Australia, 2017. PMLR.

[40] Karen Simonyan, Andrea Vedaldi, and Andrew Zisserman. Deep inside convolutional networks: Visualising image classification models and saliency maps. *Preprint arXiv:1312.6034*, 2013.

[41] Xuelin Situ, Ingrid Zukerman, Cecile Paris, Sameen Maruf, and Gholamreza Haffari. Learning to explain: Generating stable explanations fast. In *Proceedings of the 59th Annual Meeting of the Association for Computational Linguistics and the 11th International Joint Conference on Natural Language Processing (Volume 1: Long Papers)*, pages 5340–5355, 2021.

[42] Eric J Snider, Sofia I Hernandez-Torres, and Emily N Boice. An image classification deep-learning algorithm for shrapnel detection from ultrasound images. *Scientific Reports*, 12(1):1–12, 2022.

[43] Lina Song, Po-Wei Li, Yan Gu, and Chia-Ming Fan. Generalized finite difference method for solving stationary 2D and 3D stokes equations with a mixed boundary condition. *Computers & Mathematics with Applications*, 80(6):1726–1743, 2020.

[44] State of California. California consumer privacy act (CCPA). <https://oag.ca.gov/privacy/ccpa>, 2021. Online, visited on July 2023.

[45] Mukund Sundararajan, Ankur Taly, and Qiqi Yan. Axiomatic attribution for deep networks. In *International Conference on Machine Learning*, pages 3319–3328. PMLR, 2017.

[46] Sarah Tan, Giles Hooker, Paul Koch, Albert Gordo, and Rich Caruana. Considerations when learning additive explanations for black-box models. *Machine Learning*, pages 1–27, 2023.

[47] John D Towers. Finite difference methods for approximating heaviside functions. *Journal of Computational Physics*, 228(9):3478–3489, 2009.

[48] Shimon Ullman. Using neuroscience to develop artificial intelligence. *Science*, 363(6428):692–693, 2019.

[49] Joaquin Vanschoren, Jan N Van Rijn, Bernd Bischl, and Luis Torgo. OpenML: Networked science in machine learning. *ACM SIGKDD Explorations Newsletter*, 15(2):49–60, 2014.

[50] Hilde JP Weerts, Werner van Ipenburg, and Mykola Pechenizkiy. A human-grounded evaluation of SHAP for alert processing. *Preprint arXiv:1907.03324*, 2019.

[51] Maksymilian Wojtas and Ke Chen. Feature importance ranking for deep learning. *Advances in Neural Information Processing Systems*, 33:5105–5114, 2020.

[52] Mengjiao Yang and Been Kim. Benchmarking attribution methods with relative feature importance. *Preprint arXiv:1907.09701*, 2019.

[53] Muhammad Rehman Zafar and Naimul Khan. Deterministic local interpretable model-agnostic explanations for stable explainability. *Machine Learning and Knowledge Extraction*, 3(3):525–541, 2021.

## 9 Appendix

Our  $\mathbf{h}$  optimizer was designed to find a reasonable estimate of the displacement parameter  $\mathbf{h}$  when running the centered finite difference method ( $FD$ ) to compute the partial derivatives required by the T-Explainer. The optimizer is based on a binary search that minimizes a cost function of mean squared error (MSE). The optimum  $\mathbf{h}$  should be a sufficiently small value but not too small to avoid round-off errors or singularity cases and should not be too large to avoid truncation errors.

Finite differences are well-established approaches to approximate differential equations, replacing the derivatives with discrete approximations (such transformation results in computationally feasible systems of equations) [27].

The algorithm 1 provides high-level details about the optimization process to estimate the parameter  $\mathbf{h}$ . If  $\mathbf{h}$  leads to a singular or rank-deficient Jacobian matrix, the final  $\nabla f_{\mathbf{x}}$  will lead the T-Explainer to attribute misleading null values to potentially important features. Then,  $\theta$  is a function that keeps the numerical stability by checking if the gradient of  $f$  comes from a non-singular (or full-rank) matrix.

---

**Algorithm 1** The  $\mathbf{h}$  optimizer. The input parameter  $max\_itr$  defines the maximum number of iterations.

---

**Input:**  $f, \mathbf{x}, h_{min}, h_{max}, max\_itr$   
**Parameter:**  $C$ , a constant value independent of  $\mathbf{h}$  [27]  
**Output:** The optimum  $\mathbf{h}$  and estimated  $\nabla f_{\mathbf{x}}$

```

1: Let  $h_{left} \leftarrow h_{min}$ ,  $h_{right} \leftarrow h_{max}$ ,  $prev\_cost \leftarrow 1$ 
2:  $in\_loop \leftarrow$  True,  $itr \leftarrow 0$ 
3: while  $in\_loop$  is True do
4:    $itr \leftarrow itr + 1$ 
5:    $f_{\mathbf{x}} \leftarrow f(\mathbf{x})$ 
6:    $\mathbf{h} \leftarrow (h_{left} + h_{right})/2$ 
7:    $\epsilon_{\mathbf{x}} \leftarrow C * (h_{left})^2$ 
8:    $\nabla f_{\mathbf{x}} \leftarrow FD(f, \mathbf{x}, \mathbf{h})$ 
9:    $\tilde{f}_{\mathbf{x}} \leftarrow f(\mathbf{x} + \mathbf{h}) - \nabla f_{\mathbf{x}} \cdot \mathbf{h}$ 
10:   $curr\_cost \leftarrow \mathcal{L}(f_{\mathbf{x}}, \tilde{f}_{\mathbf{x}})$ 
11:  if  $curr\_cost > \epsilon_{\mathbf{x}}$  then
12:     $h_{right} \leftarrow \mathbf{h}$ 
13:  else
14:    if  $\theta(\nabla f_{\mathbf{x}})$  is True then
15:       $h_{left} \leftarrow \mathbf{h}$ 
16:    else if  $prev\_cost$  and
         $|curr\_cost - prev\_cost| < \epsilon_{\mathbf{x}}$  then
17:       $in\_loop \leftarrow$  False
18:    else
19:       $h_{left} \leftarrow \mathbf{h}$ 
20:    end if
21:  end if
22:   $prev\_cost \leftarrow curr\_cost$ 
23:  if  $itr > max\_itr$  then
24:     $in\_loop \leftarrow$  False
25:  end if
26: end while
27: return  $\mathbf{h}$  and  $\nabla f_{\mathbf{x}}$ 

```

---